J|A|C|S
ARTICLES
Published on Web 06/01/2006

X-ray Illumination Induced Fe(II) Spin Crossover in the Prussian Blue Analogue Cesium Iron Hexacyanochromate

Dionisis Papanikolaou,[†] Serena Margadonna,[‡] Wataru Kosaka,[||] Shin-ichi Ohkoshi,[||] Michela Brunelli,[§] and Kosmas Prassides*,[†]

Contribution from the Department of Chemistry, University of Durham, Durham DH1 3LE, UK, the School of Chemistry, University of Edinburgh, Edinburgh EH9 3JJ, UK, the Department of Applied Chemistry, School of Engineering, University of Tokyo, 7-3-1 Hongo, Bunkyo-ku, Tokyo 113-8656, Japan, and the European Synchrotron Radiation Facility, 38042 Grenoble, France

Received March 17, 2006; E-mail: K.Prassides@durham.ac.uk

Abstract: The effect of X-ray illumination on the structural properties of the mixed valence Prussian blue analogue $CsFe^{II}[Cr^{III}(CN)_6]$ has been studied by time-dependent high-resolution synchrotron X-ray diffraction. Abrupt isosymmetric phase transitions, accompanied by dramatic volume collapse, were found in the temperature range 245−265 K, induced by sudden Fe^{II} spin transitions from the high spin (HS) ($^4t_{2g}^2e_g$, $S = 2$) to the low spin (LS) ($^6t_{2g}^0e_g$, $S = 0$) configuration. Absorption of X-ray photons generates photoexcited Fe^{II}(LS) domains whose size rapidly grows with time until the percolation threshold is reached and the structure collapse is triggered. The persistent character of the optically excited spin crossover states derives from the strong electron−phonon coupling, associated with the large lattice relaxations, which accompany the internal spin rearrangements. It is thus possible to use X-ray light in a controllable and efficient way to induce photoswitching between the ground and hidden or inaccessible excited states in suitably selected multistable materials in the bulk.

Introduction

The exploration of the effects of external perturbations (temperature, pressure, magnetic and electric fields, light irradiation) on the structural, electronic, and magnetic properties of materials is a key area of research in contemporary chemistry. In particular, manipulation of matter by light can lead to optically induced phase transitions, as appropriate atomic or molecular units are selectively photoexcited and through some cooperative interaction can condense in a new structure with different electronic and/or magnetic properties. The density of photoexcited units depends on the excitation power and their relaxation time, and photoinduced phase transitions typically occur at a critical value of the excitation power. Prominent examples of photoinduced switching between available spin states have been observed in bistable molecular systems, such as the spin crossover complexes[1] of certain transition metal ions with between four and seven d-electrons in which light can induce a change between two metal-centered spin configurations and thereby alter drastically the optical and magnetic properties. This effect is widely known as light-induced excited spin state trapping (LIESST).[2] The spin transitions involve significant changes in the metal−ligand bond lengths and in the ligand conformations around the metal centers in the solid state. Both abrupt and continuous spin-state transitions have been observed, and these are mediated by crystallographic phase changes, by changes in molecular motion or conformation, or by more subtle intermolecular effects.[3]

Another class of switchable systems exhibiting multistability is the family of Robin−Day Class II[4] mixed valence Prussian blue analogues, $A_xM^{II}{}_y[M'^{III}(CN)_6]\cdot nH_2O$ (A = alkali metal; M and M′ = divalent and trivalent transition metal ions, respectively).[5] These also have available quasi-degenerate electronic states whose energy difference frequently approaches the thermal energy *kT*, making possible the transition between them on

[†] University of Durham.
[‡] University of Edinburgh.
[§] University of Tokyo.
[||] ESRF.

(1) (a) König, E. *Prog. Inorg. Chem.* **1987**, *35*, 527. (b) Kahn, O.; Kröber, J.; Jay, C. *Adv. Mater.* **1992**, *4*, 718. (c) Gütlich, P.; Garcia, Y.; Goodwin, H. A. *Chem. Soc. Rev.* **2000**, *29*, 419. (d) Real, J. A.; Gaspar, A. B.; Niel, V.; Muñoz, M. C. *Coord. Chem. Rev.* **2003**, *236*, 121. (e) Gaspar, A. B.; Ksenofontov, V.; Seredyuk, M.; Gütlich, P. *Coord. Chem. Rev.* **2005**, *249*, 2661.

(2) (a) Decurtins, S.; Gütlich, P.; Köhler, C. P.; Spiering, H.; Hauser, A. *Chem. Phys. Lett.* **1984**, *105*, 1. (b) Decurtins, S.; Gütlich, P.; Hasselbach, K. M.; Spiering, H.; Hauser, A. *Inorg. Chem.* **1985**, *24*, 2174. (c) Létard, J. F.; Real, J. A.; Moliner, N.; Gaspar, A. B.; Capes, L.; Cador, O.; Kahn, O. *J. Am. Chem. Soc.* **1999**, *121*, 10630.

(3) (a) Real, J. A.; Andrés, E.; Muñoz, M. C.; Julve, M.; Granier, T.; Bousseksou, A.; Varret, F. *Science* **1995**, *268*, 265. (b) Létard, J. F.; Guionneau, P.; Codjovi, E.; Lavastre, O.; Bravic, G.; Chasseau, D.; Kahn, O. *J. Am. Chem. Soc.* **1997**, *119*, 10861. (c) Boukheddaden, K.; Shteto, I.; Hôo, B.; Varret, F. *Phys. Rev. B* **2000**, *62*, 14796. (d) Herchel, R.; Boèa, R.; Gembicky, M.; Kozisek, J.; Renz, F. *Inorg. Chem.* **2004**, *43*, 4103. (e) Chernyshov, D.; Hostettler, M.; Törnroos, K. W.; Bürgi, H.-B. *Angew. Chem.* **2003**, *42*, 3825. (f) Marchivie, M.; Guionneau, P.; Létard, J. F.; Chasseau, D.; Howard, J. A. K. *J. Phys. Chem. Solids* **2004**, *65*, 17. (g) Thompson, A. L.; Goeta, A. E.; Real, J. A.; Galet, A.; Muñoz, M. C. *Chem. Commun.* **2004**, 1390.

(4) Robin, M. B.; Day, P. *Adv. Inorg. Chem. Radiochem.* **1967**, *10*, 247.

(5) (a) Dunbar, K. R.; Heintz, R. A. *Prog. Inorg. Chem.* **1997**, *45*, 283. (b) Ohkoshi, S.; Hashimoto, K. *J. Photochem. Photobiol., C* **2001**, *2*, 71. (c) Sato, O. *Acc. Chem. Res.* **2003**, *36*, 692. (d) Verdaguer, M.; Girolami, G. S. In *Magnetism: Molecules to Materials V*; Miller, J. S., Drillon, M., Eds.; Wiley-VCH: Weinheim, 2005; p 283.

10.1021/ja061650r CCC: $33.50

application of an appropriate external stimulus. Most commonly these transitions, which involve internal metal-to-metal charge transfer ($M^{II}-N-C-M'^{III} \rightarrow M^{III}-N-C-M'^{II}$) mediated by the cyanide bridge, are induced by a change in temperature,[6] but they can be also achieved by application of pressure[7] or by light irradiation.[8] Given the enormous flexibility of the cubic Prussian blue framework structure, which can accommodate a wide selection of metal ions and/or interstitial units and the outstanding ability of the cyanide bridging ligand to communicate electronic and spin information between the metal ions, a tremendous variety of internal charge-transfer processes and spin transitions have been documented in detail.[5] The strong coupling between the electronic and lattice degrees of freedom (large electron−phonon interaction) in these systems also typically triggers the occurrence of long-range cooperative structural phase transitions, as a result of the thermo-, piezo-, or photo-induced internal redox processes.

Both the spin state transitions in spin crossover complexes and the intervalence electron transfer transitions in metal polycyanides are typically induced through illumination by light (in the near-IR, visible, or UV region) whose wavelength, λ, is comparable to the Franck−Condon excitation energy between the ground and metastable excited states. Conversely, it may be possible to switch the photoinduced state back to the ground state by using light of a longer wavelength, λ'. On the other hand, phototransformations in these molecular magnetic materials induced by light of much harder energy, like X-rays, have been hitherto essentially neglected. This is to a certain extent justified, as the energy of X-ray photons (a few keV) is typically much larger than the energy difference between the ground and the various molecular metastable states (a few eV) and X-ray irradiation could lead to irreversible chemical changes in these soft materials (radiation damage). However, there has been considerable evidence from related disciplines that X-ray photoirradiation can also trigger controllable structural phase transformations involving significant changes in the conducting and magnetic properties of selected materials. For instance, X-ray light at low temperatures has been shown to drive the transition from an insulating antiferromagnetic to a metallic ferromagnetic state in the $Pr_{0.7}Ca_{0.3}MnO_3$ manganate[9] and from a charge-ordered spin dimerized to a disordered dimer state in the $CuIr_2S_4$ spinel.[10] These materials are also characterized by the existence of various competing lattice and electronic phases, and the interaction of the X-ray excited states with lattice, spin, orbital, or charge degrees of freedom can lead to bulk phase transformations.

A substantial advantage of X-ray-induced phototransformations is that, in the course of these processes, the stimulus can be simultaneously employed to act as a probe of the occurring changes of matter. For instance, as excited metastable electronic and spin states are populated and evolve with time of illumination at different conditions, time-resolved X-ray diffraction could be used for simultaneous complete structural determination and time-resolved X-ray absorption spectroscopy for metal valence states determination. Along these lines, metal-to-metal ($Co^{II}-N-C-Fe^{III} \rightarrow Co^{III}-N-C-Fe^{II}$) electron transfer was induced by X-ray irradiation at low temperatures in the Prussian blue analogue $Rb_{1.8}Co_4[Fe(CN)_6]_{3.3}\cdot 13H_2O$, and the resulting phase transformation was monitored by energy-dispersive synchrotron X-ray diffraction.[11] Similarly, the $Rb_{0.7}Mn^{II}_{1.15}[Fe^{III}(CN)_6]\cdot 2H_2O$ system proved extremely sensitive to X-ray light displaying facile interconversion between a number of excited states with differing charge (electronic) and spin (magnetic) states through both continuous (second order) and discontinuous (first order) phase transitions at temperatures ranging from 10 K to room temperature.[12] The structural relaxations of the otherwise inaccessible electronic excited states were accurately followed by high-resolution synchrotron X-ray diffraction, which allowed elucidation of the rich phase diagram in detail.

$CsFe^{II}[Cr^{III}(CN)_6]$ was recently reported to be the first member of a Prussian blue analogue series to display a thermally induced Fe^{II} (HS, $S = 2$) $\leftrightarrow$ (LS, $S = 0$) spin crossover.[13] By embedding spin crossover active centers within the versatile Prussian blue cubic architecture, this discovery opens the way for studying the spin crossover phenomenon in extended high-symmetry three-dimensional networks and for considering its coupling with a variety of additional functionalities, including magnetic order and light-induced magnetization. Here we show that X-ray light can induce conversion from the HS to the LS state of the Fe^{II} centers over a temperature range, which is not restricted to coincide with that of the thermal hysteresis loop. The cooperative nature of the spin switching triggers abrupt isostructural phase transformations in the bulk that are accompanied by large volume collapse, as evidenced by high-resolution synchrotron X-ray diffraction measurements.

Experimental Details

The $CsFe[Cr(CN)_6]$ samples used in the present work were prepared as brown crystalline powders by very slow dropwise addition of an aqueous solution of $FeCl_2$ (0.01 M)/CsCl (1 M) to an aqueous solution of $K_3[Cr(CN)_6]$ (0.01 M)/CsCl (1 M) at ambient temperature. The powders were then collected by filtration, and their stoichiometry was established by inductively coupled plasma (ICP) and standard microanalytical and thermogravimetric analysis techniques (Fe:Cr:C:N = 1:1:6:6, H_2O/formula unit < 0.1). Phase purity of the materials was confirmed by infrared spectroscopy on a Perkin-Elmer 1600 FTIR spectrometer (cyanide stretching frequency at 2161 cm^{-1}) and X-ray

(6) (a) Ohkoshi, S.; Tokoro, H.; Utsunomiya, M.; Mizuno, M.; Abe, M.; Hashimoto, K. *J. Phys. Chem. B* **2002**, *106*, 2423. (b) Bleuzen, A.; Escax, V.; Ferrier, A.; Villain, F.; Verdaguer, M.; Münsch, P.; Itié, J.-P. *Angew. Chem.* **2004**, *43*, 3728. (c) Ohkoshi, S.; Matsuda, T.; Tokoro, H.; Hashimoto, K. *Chem. Mater.* **2005**, *17*, 81.

(7) (a) Ksenofontov, V.; Levchenko, G.; Reiman, S.; Gütlich, P.; Bleuzen, A.; Escax, V.; Verdaguer, M. *Phys. Rev. B* **2003**, *68*, 024415. (b) Moritomo, Y.; Hanawa, M.; Ohishi, Y.; Kato, K.; Takata, M.; Kuriki, A.; Nishibori, E.; Sakata, M.; Ohkoshi, S.; Tokoro, H.; Hashimoto, K. *Phys. Rev. B* **2003**, *68*, 144106. (c) Hanawa, H.; Moritomo, Y.; Tateishi, J.; Ohishi, Y.; Kato, K. *J. Phys. Soc. Jpn.* **2004**, *73*, 2759. (d) Coronado, E.; Gimenez-Lopez, M. C.; Levchenko, G.; Romero, F. M.; Garcia-Baonza V.; Milner, A.; Paz-Pasternak, M. *J. Am. Chem. Soc.* **2005**, *127*, 4580. (e) Egan, L.; Kamenev, K.; Papanikolaou, D.; Takabayashi, Y.; Margadonna, S. *J. Am. Chem. Soc.* **2006**, *128*, 6034.

(8) (a) Sato, O.; Iyoda T.; Fujishima, A.; Hashimoto, K. *Science* **1996**, *272*, 704. (b) Bleuzen, A.; Lomenech, C.; Escax, V.; Villain, F.; Varret, F.; Cartier dit Moulin, C.; Verdaguer, M. *J. Am. Chem. Soc.* **2000**, *122*, 6648. (c) Pejakovic, D. A.; Manson, J. L.; Miller, J. S.; Epstein, A. J. *Phys. Rev. Lett.* **2000**, *85*, 1994. (d) Rombaut, G.; Verelst, M.; Golhen, S.; Ouahab, L.; Mathonière, C.; Kahn, O. *Inorg. Chem.* **2001**, *40*, 1151. (e) Tokoro, H.; Ohkoshi, S.; Hashimoto, K. *Appl. Phys. Lett.* **2003**, *82*, 1245. (f) Arimoto, Y.; Ohkoshi, S.; Zhong, Z. J.; Seino, H.; Mizobe, Y.; Hashimoto, K. *J. Am. Chem. Soc.* **2003**, *125*, 9240. (g) Herrera, J. M.; Marvaud, V.; Verdaguer, M.; Marrot, J.; Kalisz, M.; Mathonière, C. *Angew. Chem.* **2004**, *43*, 2.

(9) Kiryukhin, V.; Casa, D.; Hill, J. P.; Keimer, B.; Vigliante, A.; Tomioka, Y.; Tokura, Y. *Nature* **1997**, *386*, 813. Cox, D. E.; Radaelli, P. G.; Marezio, M.; Cheong, S.-W. *Phys. Rev. B* **1998**, *57*, 3305.

(10) Ishibashi, H. T.; Koo, Y.; Hor, Y. S.; Borissov, A.; Radaelli, P. G.; Horibe, Y.; Cheong, S.-W.; Kiryukhin, V. *Phys. Rev. B* **2002**, *66*, 144424.

(11) Escax, V.; Bleuzen, A.; Itie, J. P.; Munsch, P.; Varret, F.; Verdaguer, M. *J. Phys. Chem. B* **2003**, *107*, 4763.

(12) Margadonna, S.; Prassides, K.; Fitch, A. N. *Angew. Chem.* **2004**, *43*, 6316.

(13) Kosaka, W.; Nomura, K.; Hashimoto, K.; Ohkoshi, S. *J. Am. Chem. Soc.* **2005**, *127*, 8590.

powder diffraction on a Bruker D8 Advance diffractometer using freshly prepared samples. As it soon became apparent that the quality of the samples gradually deteriorated on standing at ambient temperature, all measurements reported in this work were performed on powders cooled to below 270 K immediately after preparation.

Magnetization measurements were performed at 0.5 T on a 10.3-mg sample in the temperature range 1.8−270 K at a heating/cooling rate of 0.5 K min^{-1} with a Quantum Design SQUID magnetometer. Total magnetic susceptibilities were obtained after correcting for the diamagnetic core contributions. Variable temperature X-ray diffraction data were collected with a Bruker AXS D8 Advance diffractometer equipped with a Cu tube, a Ge(111) incident beam monochromator (λ = 1.5406 Å), and a Vantec-1 position sensitive detector. The powdered sample was mounted on an amorphous silica disk. The data were collected over a temperature range of 270−16−270 K. Measurements (152 in total) were recorded over 40 h (every 5 K, 19 min each, a 0.3 K min^{-1} heating/cooling rate between temperatures, a 2θ range of 5°−70°, and a step time of 0.25 s). The data were rebinned onto a step size of 0.017° for Rietveld analysis with the Topas Academic suite of programs.[14] For the angle-dispersive high-resolution synchrotron X-ray diffraction measurements, samples were sealed in thin-wall glass capillaries 0.5 mm in diameter. With the sample inside a continuous-flow cryostat, synchrotron X-ray powder diffraction data (λ = 0.851 26 Å, E = 14.565 keV, beamsize approximately 1 × 1 mm^2, photon flux on sample ~10^{13} photons s^{-1}) were collected on heating at 100, 245, and 265 K in continuous scanning (4°/min) mode as a function of illumination time using the high-resolution multianalyzer powder diffractometer on beamline ID31 at the European Synchrotron Radiation Facility (ESRF), Grenoble, France. The data were rebinned in the range 7°−45° to a step of 0.005°, and local ESRF software were employed to extract full diffraction patterns for predefined time intervals, Δt. Analysis of the synchrotron X-ray diffraction profiles was performed with the GSAS suite of Rietveld analysis programs.[15]

Results

Temperature Dependence of the Structural and Magnetic Properties. Figure 1a shows the temperature evolution of the magnetic susceptibility data for $CsFe[Cr(CN)_6]$ displayed as the product χT vs T. At 270 K, χT = 6.05 cm^3 K mol^{-1} in excellent agreement with the earlier assignment of the spin and oxidation states of the metal ions as Fe^{II}(HS, S = 2, $^4t_{2g}{}^2e_g$)−Cr^{III}(S = $^3/_2$, $^3t_{2g}{}^0e_g$).[13] On cooling, χT shows an abrupt change below 212 K toward a local minimum of 2.60 cm^3 K mol^{-1} at 190 K, consistent with a thermally induced first-order phase transition driven by the crossover of the Fe^{II} spin state to give Fe^{II}(LS, S = 0, $^6t_{2g}{}^0e_g$)−Cr^{III}(S = $^3/_2$, $^3t_{2g}{}^0e_g$) units. The Fe^{II} HS→LS spin crossover is reversible but strongly hysteretic as, on heating, χT abruptly increases above 241 K (width of the thermal hysteresis loop, $\Delta T_{h,m}$ = 37 K).

The change in the magnetic properties is accompanied by large lattice relaxations, which are clearly reflected in the temperature evolution of the structural properties. At 268 K, the crystal structure of $CsFe[Cr(CN)_6]$ is face-centered cubic (*fcc*) with a lattice constant, a = 10.7113(5) Å. On cooling below 219 K, the intensities of the Bragg reflections of the Fe^{II} HS phase begin to decrease rapidly, while, at the same time, a new set of reflections shifted to higher angles begins to grow. The transformation to the contracted Fe^{II} LS phase, which is also *fcc*, is complete within 15 K, and no further changes take place down to 16 K (a = 10.3375(5) Å at 204 K). On heating,

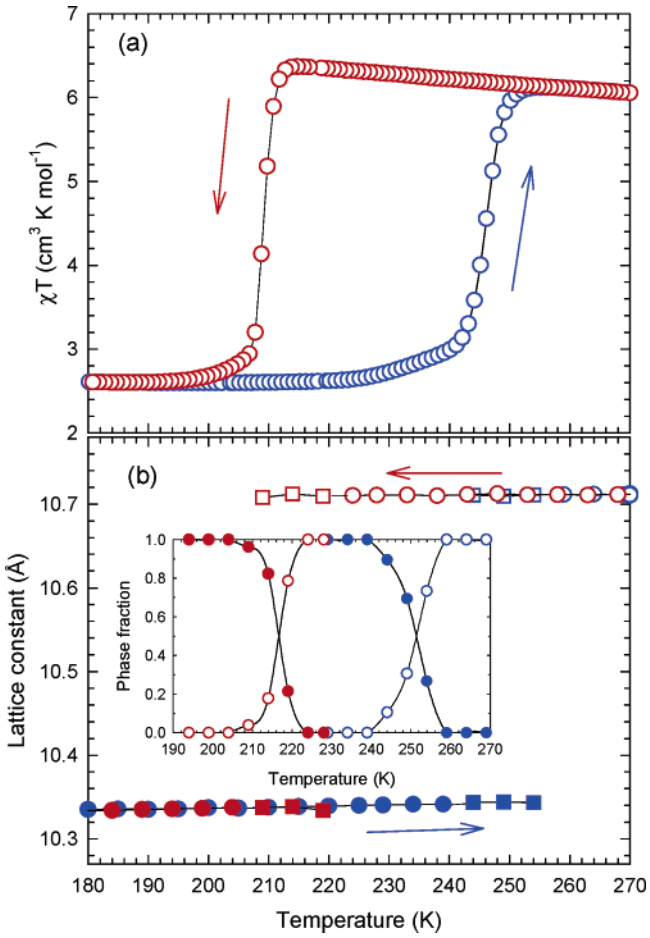

Figure 1. Temperature dependence (a) of the product of the magnetic susceptibility times temperature, χT (H = 0.5 T, red open circles: cooling, blue open circles: heating) and (b) of the cubic lattice constants of the Fe^{II} HS and LS phases (red circles/squares: cooling, blue circles/squares: heating; open circles: HS phase, full circles: LS phase, squares: two-phase coexistence) of $CsFe^{II}[Cr^{III}(CN)_6]$. The *inset* in (b) shows the temperature evolution of the HS and LS phase fractions for both cooling and heating protocols.

the structural response of the LS phase mirrors exactly the behavior observed in the magnetic susceptibility measurements with the onset of the LS→HS phase transition now occurring at 244 K (width of the thermal hysteresis loop in the lattice constant measurements, $\Delta T_{h,l}$ = 35 K). Figure 1b shows the detailed temperature dependence of the cubic lattice constants and phase fractions of the two phases, as extracted from Rietveld refinements of the diffraction profiles employing the $Fm\bar{3}m$ space group (vide infra). The decrease in the unit cell volume through the HS ↔ LS phase transition is −10.1(2)%. The calculated thermal expansivities, α_a (= dln a/dT) are positive for both phases (11.4(2) and 3.2(8) ppm K^{-1} for the LS and HS structures, respectively) and do not reveal any unusual thermal behavior.[16]

Synchrotron X-ray Diffraction Measurements. We first examined the synchrotron X-ray diffraction profile of the Fe^{II} LS phase of $CsFe[Cr(CN)_6]$ collected at 100 K after cooling without X-ray illumination. No reflections violating *fcc* extinction rules are evident, and the crystal structure is strictly cubic. Rietveld analysis proceeded smoothly with the generic structural

(14) Topas Academic: http://pws.prserv.net/Alan.Coelho/.
(15) Larsen, A. C.; von Dreele, R. B. GSAS software, LANL Report No. LAUR 86-748.
(16) Margadonna, S.; Prassides, K.; Fitch, A. N. *J. Am. Chem. Soc.* **2004**, *126*, 15390.

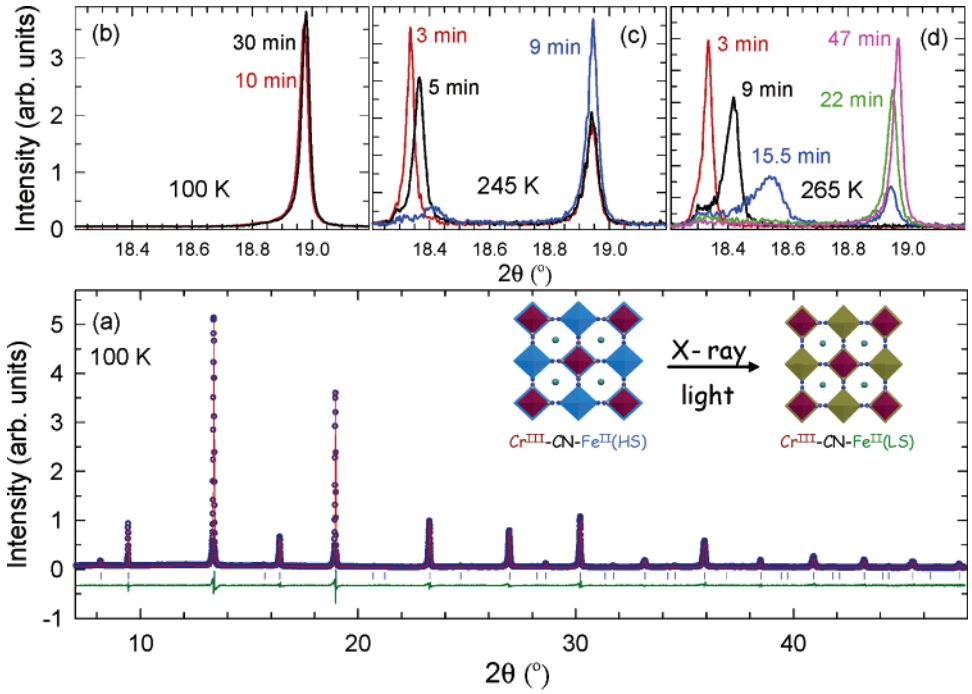

Figure 2. (a) Final observed (○) and calculated (—) synchrotron X-ray powder ($\lambda = 0.851\ 26$ Å) diffraction profiles for $CsFe[Cr(CN)_6]$ at 100 K after 10 min of X-ray illumination. The lower solid line shows the difference profile, and the tick marks show the reflection positions. (b−d) Selected region of representative diffraction profiles showing the evolution of the (222) Bragg reflection with increasing X-ray ($E = 14.565$ keV) illumination time: (b) 100 K, (c) 245 K, (d) 265 K. Each curve is labeled with the corresponding illumination time. The *inset* in (a) depicts schematically the X-ray induced rearrangement of the Prussian blue structural building block.

Table 1. Refined Structural Parameters of the LS Phase for $CsFe[Cr(CN)_6]$ at 100 K after 10 min of X-ray Illumination[a]

	n	*x*	*y*	*z*	position	B_{iso} (Å^2)
Cr	1	0	0	0	4a	1.05(5)
Fe	1	$^1/_2$	$^1/_2$	$^1/_2$	4b	1.05(5)
Cs	0.5	$^1/_4$	$^1/_4$	$^1/_4$	8c	1.78(5)
C	1	0.204 38(4)	0	0	24e	0.67(7)
N	1	0.312 92(6)	0	0	24e	0.67(7)

[a] Estimated errors in the last digits are given in parentheses. The space group is $Fm\bar{3}m$. The X-ray wavelength is 0.851 26 Å. The refined lattice constant is $a = 10.324\ 31(3)$ Å. The agreement factors are $R_{wp} = 9.73\%$ and $R_{exp} = 4.77\%$.

Table 2. Selected Distances (Å) of the $[Fe^{II}(NC)_6]^{4-}$ Octahedra in $CsFe[Cr(CN)_6]$ as a Function of X-ray Illumination Time at Different Temperatures[a]

temp (K)	illumination time (min)	Fe^{II}(LS)–N (Å)	Fe^{II}(HS)–N (Å)
100	10	1.9315(8)	
245	1.33	1.9409(14)	2.1148(14)
245	23	1.9377(13)	
265	1.33		2.1153(12)
265	49	1.9340(13)	

[a] The Cr^{III}−C distances of the $[Cr^{III}(CN)_6]^{3-}$ octahedra remain unchanged at 2.110(1) Å.

model of mixed valence Prussian blue analogues,[17] comprising a three-dimensional network of $Fe(NC)_6$ and $Cr(CN)_6$ octahedra bridged by the CN ligands. The results of the final refinement are shown in Figure 2a (space group $Fm\bar{3}m$, $a = 10.324\ 31(3)$ Å at 100 K; agreement factors: $R_{wp} = 9.73\%$, $R_{exp} = 4.77\%$) with fitted parameters listed in Table 1. The Fe^{II}−N and Cr^{III}−C bond distances of the $Fe(NC)_6$ and $Cr(CN)_6$ octahedra refine to 1.9315(8) and 2.1100(5) Å, respectively (Table 2), consistent with the Fe^{II}(LS)−NC−Cr^{III} assignment of the metal valence and spin states. Because of its stoichiometric nature and the absence of any hydration water molecules, $CsFe[Cr(CN)_6]$ is an unusual member of the Prussian blue family with no vacant $Cr(CN)_6$ sites in the unit cell. Moreover, we also find that the Cs^+ ions are statistically disordered (fractional occupancy = 0.5) in the tetrahedral interstitial 8*c* sites ($^1/_4$,$^1/_4$,$^1/_4$) of the framework structure.[18] We then followed the evolution of the diffraction profile at 100 K with increasing exposure time to the X-ray light. No significant changes were evident in either the position or the intensity/width of the diffraction peaks for a period of 90 min (Figure 2b) implying that the LS phase is robust to illumination by X-ray light.

The $CsFe[Cr(CN)_6]$ sample was then heated in the dark to 245 K. At this temperature, the material has partially transformed to the HS phase, and the recorded synchrotron X-ray diffraction profile is consistent with coexisting LS and HS phases (phase fractions: 42.6(2)% and 57.4(2)%, respectively). However, the response of the material at this temperature to continued exposure to the X-ray beam is very pronounced. A striking feature of the data at 245 K is that, although the structure remains cubic, all diffraction peaks associated with the expanded HS phase continuously broaden and shift to higher angles

(17) Buser, H. J.; Schwarzenbach, D.; Petter, W.; Lüdi, A. *Inorg. Chem.* **1977**, *16*, 2704.

(18) The alternative structural model with preferential ordering of the Cs^+ ions in half of the available tetrahedral interstices (sites 4*c* ($^1/_4$,$^1/_4$,$^1/_4$) or 4*d* ($^3/_4$,$^3/_4$,$^3/_4$)) to give the noncentrosymmetric space group $F\bar{4}3m$ can be unambiguously discarded in the present case, as the Rietveld refinement described the synchrotron X-ray diffraction profile very poorly with a much inferior agreement factor ($R_{wp} = 57.6\%$) and severe disagreement between calculated and observed intensities. In fact, there is a prevailing empirical rule in the Prussian blue literature that systems with stoichiometry AM-$[M'(CN)_6]$ containing the large Rb^+ or Cs^+ supporting cations invariably adopt the $F\bar{4}3m$ space group. While this may well be true in many cases, like $RbMn[Fe(CN)_6]$,[6a] the present structural results on $CsFe[Cr(CN)_6]$ imply that it is not universal.

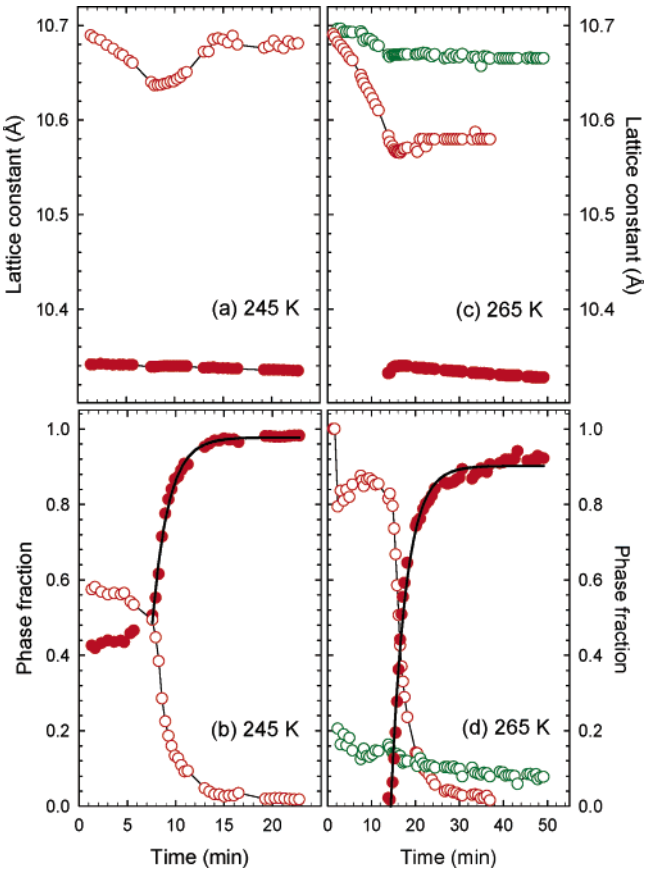

Figure 3. Evolution with increasing X-ray illumination time of (a and c) the cubic lattice constants and (c and d) the phase fractions of the Fe^{II} HS and LS phases (open circles: HS phase, full circles: LS phase) for $CsFe[Cr(CN)_6]$ at 245 and 265 K, respectively. The solid lines in (c) and (d) represent best fits to the Avrami equation of growth (see text).

(Figure 2c), implying a rapid contraction at a rate of 2.31(2) $Å^3$ min^{-1} (Figure 3a) and an overall volume decrease of 0.82(3)% after 6 min of illumination. In contrast, the Bragg reflections of the LS phase are hardly affected in the course of the experiment. Rietveld refinements employing a two-$Fm\bar{3}m$-phase structural model reveal a monotonic decrease of the Fe^{II}(HS)−N bond distance from 2.1148(14) to 2.1002(12) Å after ∼6 min of exposure of the sample to the X-ray beam. Following this incubation period, *all* diffraction peaks of the HS phase suddenly begin to diminish in intensity very rapidly, while those of the LS phase begin to grow. This provides the signature of a sudden transformation of the HS structure to the isostructural LS one with drastically reduced lattice dimensions (Figure 3a). The fraction of the LS phase grows rapidly in a very short time, and the bulk transformation is essentially complete within an additional ∼6 min of illumination. The abrupt collapse in the unit cell metrics ($\Delta V/V \approx -9.55(3)\%$) can be understood in terms of an X-ray induced spin crossover process Fe^{II}(HS) → Fe^{II}(LS), which occurs very efficiently at this temperature. A notable feature of the time evolution of the lattice constant of the untransformed HS phase is that in the course of the X-ray induced HS → LS phase transition it gradually recovers to its value before illumination. The observed photoinduced effects are of persistent nature. Upon switching off the X-ray beam and warming the sample in the dark to 265 K, the LS phase survives (phase fraction: 87%), which implies that the lattice strains accompanying the spin crossover are large enough that relaxation does not occur immediately even at temperatures outside the thermal hysteresis loop.

Substantial changes to the diffraction profile of $CsFe[Cr(CN)_6]$ are also observed at 265 K (Figure 2d). At this temperature, the recorded synchrotron X-ray diffraction profile is consistent with the material being exclusively in the HS phase before illumination. However, as soon as the X-ray light is switched on, an extremely rapid change sets in and the lattice size rapidly contracts at a rate of 2.91(1) $Å^3$ min^{-1} (Figure 3c), leading to a continuous decrease of the Fe^{II}(HS)−N bond distance from 2.1153(12) to 2.0616(12) Å and of the unit cell volume by 2.98(3)% after 14 min of illumination. This process is also accompanied by a pronounced broadening of the Bragg reflections. The incubation period is longer than that observed at 245 K, but then the unit cell metrics suddenly collapse and an isostructural first-order phase transition to the LS phase again takes place. This is accompanied by a notable sharpening of the diffraction peaks, indicating the occurrence of a phase transition in the bulk. Within an additional time of ∼15 min, the X-ray induced phototransformation is essentially complete (Figure 3d), and the refined Fe^{II}−N bond distances (1.9371(17) Å) are consistent with the Fe^{II} metal centers being in the LS state. However, we note that, throughout the course of the HS → LS crossover process, a minority fraction of the material with a lattice size comparable to that of the pristine HS phase coexists. This displays a much weaker sensitivity to the X-ray beam as its fraction diminishes only very slowly with illumination time, eventually reaching ∼7.8% after 50 min.

Discussion

$CsFe^{II}[Cr^{III}(CN)_6]$ is a unique system among those exhibiting the effect of thermally induced spin crossover. Unlike the large family of spin crossover complexes, which comprise isolated molecular units, the spin active $[Fe^{II}(NC)_6]^{4-}$ centers are incorporated in the extended Prussian blue framework structure. The cubic symmetry of the latter is optimal to allow facile characterization of the structural relaxations, which should accompany any spin transformations under the application of external perturbations (temperature, pressure, and light).

The synchrotron X-ray diffraction data collected at 100 and 265 K show the presence of single-phase materials with small and large unit cell volumes, respectively. Rietveld refinements provide unambiguous evidence that the difference in lattice dimensions is entirely associated with the length of the Fe^{II}−N bonds in the two phases (1.9315(8) Å at 100 K and 2.1153(11) Å at 265 K) with the Cr^{III}−C bond distances remaining essentially the same (2.1100(5) Å at 100 K and 2.1099(7) Å at 265 K) (Table 2). This is consistent with the magnetic data and the conclusion that the isostructural phase transition is driven by a HS → LS crossover of the $[Fe^{II}(NC)_6]^{4-}$ units. The first-order nature of the transition is confirmed by the observation that, at 245 K, the two phases are in coexistence.

Experiments monitoring the effect of exposure to X-ray light have revealed that, while the LS phase is robust at both 100 and 245 K, well-defined structural rearrangements of the expanded HS phase are evident at 245 and 265 K. To develop a picture of the photoinduced effects emerging from the present synchrotron X-ray powder data, we focus on the time evolution of the diffraction profiles. At both temperatures, the phase transformation associated with the collapse of the HS into the

Table 3. Kinetic Rate Parameters for the X-ray Induced Fe^{II} HS → LS Transformation in $CsFe[Cr(CN)_6]$; the Experimental Data Were Fitted to the Avrami Rate Expression, $\alpha = 1 - \exp[-(k(t - t_0))^m]$

temp (K)	incubation time, t_0 (min)	order, m	rate constant, k (10^{-3} s^{-1})	half-life (s)
245	6.4	1.0	10.0(4)	74
265	14.0	1.0	4.9(2)	164

LS phase is rather complex and develops in time through two well-defined processes. The first process manifests itself in early times with the gradual decrease of the unit cell size. This is consistent with a progressive generation of Fe^{II}(LS)−N centers with increased X-ray illumination time and shrinking of the Fe^{II}−N bonds upon the HS−LS crossover. At the same time, the chromium coordination sphere changes very little. Though there is no unique real-space description of this effect, the observation that the width of the diffraction peaks also progressively increases (Figure 2b and 2c) leads us to describe the observed X-ray induced effect as a process of phase segregation through the formation of Fe^{II}(LS)−N islands with a local structure different from that of the average bulk structure. As the fraction of the photoconverted units increases with time, the domains progressively grow in size within the matrix of the Fe^{II}(HS)−N units. Following an incubation time, t_0, the percolation threshold is reached, and a cooperative first-order phase transformation to the bulk LS phase is abruptly triggered.

The kinetics of the X-ray photoconversion show characteristic differences between the two temperatures at which the experiments were performed. The data were analyzed with the general Avrami rate expression[19] for nucleation growth reactions, $\alpha = 1 - \exp[-(k(t - t_0))^m]$, where α is the extent of the reaction (i.e., the fraction of the photogenerated LS phase in our case), k, the rate constant, m, the order of the reaction, and t_0, the initiation time. The results of the least-squares fits of the Avrami expression to the experimental data are given in Table 3, and the fits are included in Figure 3b and 3d. The transition at both temperatures occurs very rapidly with a half-life on the order of 1−3 min and a rate equation which obeys first-order kinetics and is consistent with a diffusion controlled model of three-dimensional growth and a decreasing nucleation rate with increasing time.[19] As the LS phase is stabilized relative to the HS phase on cooling, the X-ray induced effects are similarly accelerated and the rate constant doubles between 265 and 245 K. In addition, the incubation time, t_0, before the first-order transition sets in is significantly shorter at 245 K (6.4 min) than that at 265 K (14.0 min). This can be understood if we assume that, at 245 K where both phases coexist, there are pre-existing inhomogeneities, associated with trapped LS clusters in the HS phase and vice versa. The presence of such preformed defects should be responsible for reaching the percolation threshold for the X-ray induced photoconversion at a shorter time.

Finally, we comment on the possible mechanism of the X-ray induced spin crossover. Clearly the energy of the X-ray excitation is orders of magnitude larger than the energies of the absorption bands involving either the $^1A_{1g}$ (LS) or the $^5T_{2g}$ (HS) state that are utilized in the spin crossover processes driven by resonant visible light illumination. Nonetheless the occurrence of first-order transitions involving the bulk of the sample implies a large cross section for the X-ray photoconversion. Presumably irradiation by the beam leads to the generation of X-ray photoelectrons, accompanied by the creation of core holes which are subsequently de-excited via a series of Auger processes. Once the electrons are photoexcited out of the HS state, a local defect with an accompanying lattice distortion is generated. It then appears that the recapture cross section is very small with de-excitation occurring preferentially into the LS state. The reason for this should be the dominant role of electron−phonon interactions, as in the present insulating material screening of the core holes implies polarization of the local environment. Electron−phonon interactions are stronger in the LS phase ($r(Fe^{II}(LS)-N) - r(Cr^{III}-C) \approx 0.17$ Å, $r(Fe^{II}(HS)-N) - r(Cr^{III}-C) \approx 0.01$ Å) and therefore favor its growth at the expense of the HS phase as the concentration of photogenerated local defects increases. Along these lines, we also note the persistent character of the photoinduced transition at 245 K that can be rationalized in terms of the large lattice relaxations, which accompany the spin rearrangement (strong electron−phonon coupling) and need large energies in order to be annealed. Finally, another effect that may be of relevance here stems from the very high energy of the incident X-ray photons, namely the creation of phonons due to the recoil effect.[20]

Conclusions

In conclusion, we have discovered that the mixed valence Prussian blue analogue $CsFe[Cr(CN)_6]$ is extremely sensitive to illumination by X-ray light. Time-dependent synchrotron X-ray diffraction studies were concurrently employed to follow accurately the evolution of the cubic crystal structure in the course of the phototransformations. The abrupt isosymmetric phase transitions, which are accompanied by a large volumetric contraction, are unambiguously of magnetic origin with strong coupling between the spin and lattice degrees of freedom. The absorption of X-ray photons causes the sudden conversion of the $Fe^{II}(^4t_{2g}^2e_g$, HS) centers incorporated within the Prussian blue structure to the smaller $Fe^{II}(^6t_{2g}^0e_g$, LS), while the Cr^{III}-($^3t_{2g}$) centers of the Fe^{II}−NC−Cr^{III} structural motif remain robust. The temperature range over which these effects are encountered is not restricted to temperatures coincident with the thermal hysteresis loop of the magnetic susceptibility but extends to higher temperature with the rate of the HS → LS conversion decreasing with increasing temperature. The present work has shown that X-ray light is a useful and extremely efficient stimulus to generate optically excited states of matter in an essentially quantitative way in the bulk by rapid spin photoswitching.

Acknowledgment. We thank the ESRF for provision of synchrotron X-ray beamtime and the Daiwa Foundation for financial support.

JA061650R

(19) (a) Avrami, M. *J. Chem. Phys.* **1939**, *7*, 1103. (b) Hulbert, S. F. *J. Br. Ceram. Soc.* **1969**, *6*, 11.

(20) Fujikawa, T.; Suzuki, R,; Kövér, L. *J. Electron Spectrosc. Relat. Phenom.* **2006**, *151*, 170.